

Switchable Quantum Anomalous Hall state in a strongly frustrated lattice magnet

Jörn W.F. Venderbos,¹ Maria Daghofer,¹ Jeroen van den Brink,¹ and Sanjeev Kumar²

¹*IFW Dresden, P.O. Box 27 01 16, D-01171 Dresden, Germany*

²*Indian Institute of Science Education and Research (IISER) Mohali, Knowledge city, Sector 81, Mohali 140306, India*

We establish that the interplay of itinerant fermions with localized magnetic moments on a checkerboard lattice leads to magnetic flux-phases. For weak itineracy the flux-phase is coplanar and the electronic dispersion takes the shape of graphene-like Dirac fermions. Stronger itineracy drives the formation of a non-coplanar, chiral flux-phase, in which the Dirac fermions acquire a topological mass that is proportional to a ferromagnetic spin polarization. Consequently the system self-organizes into a ferromagnetic Quantum Anomalous Hall state in which the direction of its dissipationless edge-currents can be switched by an applied magnetic field.

PACS numbers: 71.27.+a , 73.43.-f, 71.10.-w , 75.10.-b

Introduction.— The study of topologically non-trivial states of matter is one of the hottest topics in present day condensed matter physics. An understanding of topological states requires a theoretical paradigm that goes far beyond the concept of global symmetry breaking that has originally been laid out by Landau. It is remarkable that the theoretical predictions on the existence of various topologically ordered states have rather swiftly led to the discovery of an entirely new class of materials, the topological insulators [1–4]. Recent pioneering experiments have confirmed the key signatures of non-trivial topology in certain materials, e.g. spin-momentum-locked undoubled Dirac fermions [5–7] and the Quantum Spin Hall (QSH) effect [8]. These topological insulators are time-reversal (TR) invariant generalizations of the first, much older, topological state of matter, the famous Integer Quantum Hall states [9, 10] that are induced by a magnetic field, which obviously breaks TR symmetry.

In a seminal work in 1988, Haldane established that a magnetic field is not required to induce states with the same topology as IQH states [11]. It was shown that adding complex hopping to a graphene-like Hamiltonian for electrons on a honeycomb lattice opens up topologically nontrivial gaps at the Dirac points, which yields a topologically ordered, insulating state, referred to as a Quantum Anomalous Hall (QAH) state. An important feature of QAH states are edge channels, in which current can run only in one direction; in contrast to QSH states, on a single edge the opposite spin channel carrying the opposite current is absent [12]. QAH states would thus allow very robust, dissipationless charge transport along edge channels, as backscattering would be completely suppressed. However, while signatures of QAH behavior have been reported in some compounds [13–15], the QAH state is the only one among these topologically insulating states that remains to be unambiguously identified in experiment.

The experimental difficulty is mirrored by the frailty of the theoretical mass-generating mechanisms for a graphene-like kinetic energy with a linear dispersion at the Fermi level. TR-symmetry breaking via (magnetic) order requires rather specific and strong longer-range Coulomb interactions [16], because the Dirac cones' vanishing density of states at the Fermi level renders interaction-driven ordered states energetically less favorable. QAH states can more readily be induced in

models with a finite density of states [17–19], especially in cases of quadratic band crossings [20], as for instance found in the checkerboard lattice, which exhibit a weak-coupling instability [20–22]. Another approach has been to consider spin-orbit coupled magnetic semi-conductors [23] or spin-polarized QSH states [12].

Our starting point is instead the Kondo lattice model, which provides the most general context for the study of the interplay between localized spins and itinerant electrons. We will show that, depending on parameters, its ground state on the checkerboard lattice can feature massless Dirac cones or a chiral QAH state. Moreover, because the spin texture underlying the QAH state has a net ferromagnetic (FM) moment, we have a direct switching mechanism between ground-states with different chirality just by flipping the FM polarization. The ensuing possibility to reverse the direction of an edge current by an external magnetic field is an attractive feature in the context of spintronics.

In particular we focus on the case of electrons strongly coupled to large localized spins that in turn interact via a strongly frustrated antiferromagnetic superexchange. In the absence of charge carriers, the magnetic interactions give rise to a highly degenerate ground state manifold (GSM) comprised of all spin configurations that obey certain *local* constraints, which go by the name of *spin-ice rules*, as a reference to three-dimensional spin systems that remain disordered down to the lowest temperatures like the H protons in water ice [24]. It is clear that in a frustrated spin-systems governed by ice rules, doping of itinerant charge carriers will (partly) lift the macroscopic the degeneracy of the GSM [25] because of the kinetic energy competing with the local ice-rule constraints. We will show that for not too large kinetic energies, a unique flux-phase ground-state is selected in our case, whose low-energy states are described by a massless Dirac equation. When the kinetic energy becomes stronger, enhancing the competition, these Dirac fermions acquire a topological mass, and the ferromagnetic QAH state emerges.

Model and method.— We thus consider itinerant electrons coupled to localized core spins, described by the canonical one-band double-exchange model with a competing antiferromagnetic (AFM) super-exchange interaction, on the checkerboard lattice at the density of one electron per two sites, where

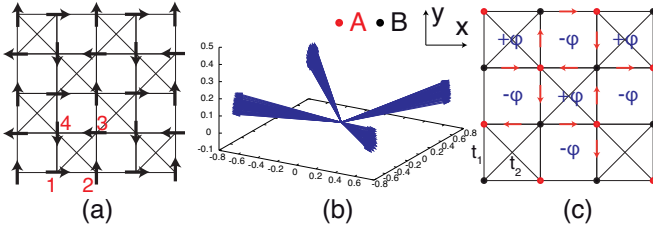


FIG. 1. (Color online) (a) Shows the localized spin texture of the “flux” phase; all spins are in plane, for number labeling see text. (b) Representation of the spins in the “umbrella” spin-chiral state, as obtained with MCMC+optimization for a 16×16 lattice with $J_{AF} = 0.105$, where $\delta = 0.148$ compared to 0.141 as would be expected analytically; all spins have been translated to a single site. (c) Staggered flux arrangement on the checkerboard lattice corresponding to this insulating umbrella phase. Red arrows indicate the gauge choice of the “gauge flux”. Note that the indicated flux threads the squares, so half of it threads the triangles.

the kinetic energy promoting ferromagnetic (FM) spin correlations is strongest. The resulting Hamiltonian is

$$H = - \sum_{\langle ij \rangle} t_{ij} (\psi_i^\dagger \psi_j + H.c.) + J_{AF} \sum_{\langle ij \rangle} \mathbf{S}_i \cdot \mathbf{S}_j, \quad (1)$$

where ψ_i^\dagger (ψ_i) creates (annihilates) a fermion on site i . Here we have assumed for simplicity that an infinite Hund’s rule perfectly aligns the fermion spin to the localized spins \mathbf{S}_i , but we have verified that the results presented in this Letter remain valid also for large but finite coupling. As the onsite spins are classical and one can take without loss of generality $|\mathbf{S}_i| = 1$, they are completely specified by polar and azimuthal angles (θ_i, ϕ_i) . As hopping and superexchange are identical along the “straight” and “diagonal” edges of the checkerboard lattice, see Fig. 1(a), both types of bonds are included in the sum over $\langle ij \rangle$. The hopping amplitude depends on the core spins as $t_{ij} = t[\cos(\theta_i/2)\cos(\theta_j/2) + \sin(\theta_i/2)\sin(\theta_j/2)e^{-i(\phi_i - \phi_j)}]$ [26]. AFM superexchange is given by J_{AF} and all energies will be measured in units of the hopping amplitude t . We use Markov Chain Monte Carlo (MCMC) simulations to treat the classical spins, where the weight of a spin configuration is given by the free energy of the effective fermionic Hamiltonian, as obtained by exact diagonalization [26]. We have performed calculations on lattices with $N = 8^2, 12^2, 16^2$, and 20^2 sites. MCMC calculations were supplemented with an energy optimization in order to suppress thermal fluctuations [27].

Checkerboard lattice magnet.— Let us first discuss the two terms in the Hamiltonian separately, corresponding to the limits $J_{AF} \rightarrow 0$ and $J_{AF} \rightarrow \infty$, and turn to them competing at the next stage. For vanishing super-exchange coupling $J_{AF} \rightarrow 0$, one finds a saturated FM state, equivalent to free spinless fermions on a checkerboard lattice. There are two bands $E_+ = 2t$ and $E_- = -2t - 4t \cos k_x \cos k_y$ and the density of states (DOS), $D(\omega) = \langle \frac{1}{N} \sum_k \delta(\omega - \epsilon_k) \rangle$, is shown in Fig. 2(a). The first Brillouin zone (BZ) is given by

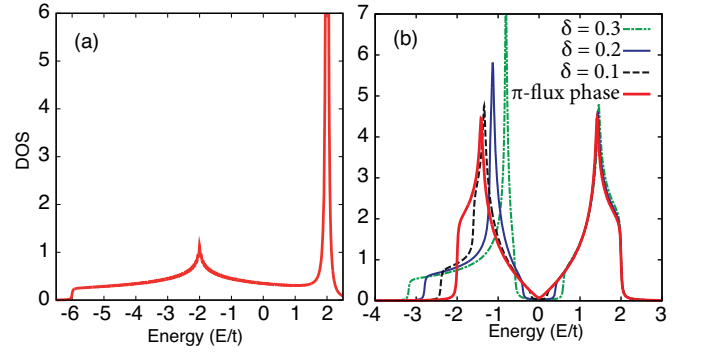


FIG. 2. (Color online) Electronic density of states of (a) the FM (spinless) phase, (b) the “flux” phase (in red) and spin-chiral umbrella phase for various δ (see text).

$(k_x, k_y) \in \{|k_x + k_y| \leq \pi\} \cap \{|k_x - k_y| \leq \pi\}$. The Heisenberg term dominating for $J_{AF} \rightarrow \infty$ is geometrically frustrated and supports an infinitely large classical degeneracy of spin ground states. This can be seen by noting that it can be rewritten in terms of the total spins on the crossed plaquettes $\mathbf{S}_{\mathcal{P}} = \mathbf{S}_1 + \mathbf{S}_2 + \mathbf{S}_3 + \mathbf{S}_4$, giving

$$J_{AF} \sum_{\langle ij \rangle} \mathbf{S}_i \cdot \mathbf{S}_j = \frac{J_{AF}}{2} \sum_{\mathcal{P}} \mathbf{S}_{\mathcal{P}} \cdot \mathbf{S}_{\mathcal{P}} - J_{AF} N, \quad (2)$$

where N is the number of sites. Clearly, the lowest energy is obtained when $\mathbf{S}_{\mathcal{P}} = 0$. This *local* requirement on the spins of each crossed square is similar to the spin-ice rule in the pyrochlore lattice. For Ising spins [28] the rule corresponds to “two up-two down”. If noncollinear spin arrangements are permitted, as we consider here, the class of states $\mathbf{S}_{\mathcal{P}} = 0$ is further increased.

For dominant super-exchange coupling $J_{AF} \gg 1$, the magnetic order is expected to belong to the highly degenerate ground-state manifold (GSM) fulfilling $\mathbf{S}_{\mathcal{P}} = 0$. The kinetic energy can leave the degeneracy intact, lift it partially or lift it completely, singling out a unique non-degenerate spin arrangement. Our MCMC calculations show that the latter is the case, the electrons pick out a particular coplanar, but not collinear, state that is schematically depicted in Fig. 1(a). Non-diagonal bonds connect orthogonal spins, while diagonal bonds connect AFM spins, effectively excluding them from the hopping term. Going around a square plaquette, the electrons pick up a phase $e^{i\pi}$, corresponding to a time-reversal invariant flux of π , and this special “flux” phase has been shown to arise in models for high- T_c superconductors [29, 30] and in the double-exchange models on the square lattice [31–34]. On the unfrustrated square lattice, it competes with the Neel state for strong J_{AF} [31–33], but since it fulfills the ice-rules, it remains stable for $J_{AF} > 0.12$ on the checkerboard lattice.

The DOS of the flux phase shows semi-metallic behaviour [see Fig. 2(b)] that originates from two Dirac points in the spectrum. Low-energy excitations are described by a relativistic Dirac equation, in full analogy with graphene [35]. The core-spin texture $\Lambda_i = (\theta_i, \phi_i)$ of the flux phase can

be written as $\Lambda_i = (\pi/2, (i-1)\pi/2)$ with $i = 1, 2, 3, 4$ [see Fig. 1(a)]. Even though the magnetic texture has a 4-site unit cell, the two-site electronic unit cell need not be enlarged. The electronic Hamiltonian, in the $(\psi_A^\dagger, \psi_B^\dagger)$ basis, is then given by $H(\mathbf{k}) = \mathbf{d}(\mathbf{k}) \cdot \boldsymbol{\sigma}$, with the Pauli matrices $\boldsymbol{\sigma} = (\sigma^x, \sigma^y, \sigma^z)$ and $\mathbf{d}(\mathbf{k}) = -(\cos k_x + \cos k_y, \cos k_x - \cos k_y, 0)$. The band structure of this state is shown in Fig. 3(a). The two inequivalent Dirac points, or valleys, are located at $\mathbf{M}_\pm = (\pm\pi/2, \pi/2)$. Expanding around the Dirac points yields an effective low-energy Hamiltonian with the two Dirac spinors $\Psi_1^\dagger = (\psi_A^\dagger(\mathbf{M}_+ + \mathbf{p}), \psi_B^\dagger(\mathbf{M}_+ + \mathbf{p}))$ and $\Psi_2^\dagger = (\psi_A^\dagger(\mathbf{M}_- + \mathbf{p}), \psi_B^\dagger(\mathbf{M}_- + \mathbf{p}))$. Rotations on momentum and spinor components bring us to the familiar form $H(\mathbf{q}) = \nu^z \otimes (q_x \sigma^x + q_y \sigma^y)$, where ν -Pauli matrices act on the valley index. This is equivalent to graphene, with two valleys around which the electrons are described by the Dirac equation and an interesting mapping exists between graphene and the flux phase [36]. One important difference to graphene is that we have here no spin degeneracy, as the spin degree of freedom was integrated out by tying the fermion spin to the core spins.

Massive QAH Dirac fermions.— Having established that a not-too-large electronic kinetic energy selects a unique non-collinear pattern for the checkerboard double-exchange magnet, which has a graphene-like Dirac spectrum, we consider next what happens upon an increase of the itineracy. Lowering J_{AF} , we find that the magnetic interactions enforcing the tetrahedron rules are overcome by the electronic kinetic energy for $J_{AF} \lesssim 0.12$. The transition is continuous and can be understood as a tilting of the flux-pattern out of the plane, forming an “umbrella”. An example is shown in Fig. 1(b): the spins fall along four directions, whose projections onto the x - y plane mirror the “flux”-phase pattern, but there is an additional FM component along the z axis. The spins can be described using an Ising variable $s = \pm 1$ (which will turn out to correspond to a scalar spin chirality) and a continuous parameter δ giving the tilting along $\mp z$: $\{\Lambda_i^s(\delta)\} = (\pi/2 + \delta, s(i-1)\pi/2)$, where $i = 1, 2, 3, 4$ again runs around a crossed plaquette. A similar scenario, but involving a more complex 8-site unit cell and leading to Chern numbers ± 2 , arises on a square lattice with longer-range couplings when nearest-neighbor hoppings are strongly modulated [34].

The scalar spin chirality of the state is defined as $\chi = \sum_{\mathcal{T}} \mathbf{S}_i \cdot \mathbf{S}_j \times \mathbf{S}_k$, where the sum is over all triangles \mathcal{T} of the checkerboard lattice, and $\mathbf{S}_i \cdot \mathbf{S}_j \times \mathbf{S}_k$ is taken in the counter-clockwise direction. The chirality as function of δ is plotted in the inset of Fig. 2(b) for umbrella states Λ^\pm , it is $\chi \approx -s\delta$ for small δ . The label $\pm s$ decides the sign of the chirality for $\delta > 0$ and is related to a (counter-)clockwise rotation of the spin projection onto the x - y plane. The umbrella states, in addition to a continuous spin rotation symmetry, thus also break a discrete \mathbb{Z}_2 symmetry. Since breaking a discrete symmetry in $2D$ is possible at finite temperature, this opens up the possibility for chiral ordering in absence of long-range magnetic ordering [37].

The effect of the tilting on the electronic degrees of freedom is to break time-reversal symmetry, as fluxes through elementary plaquettes are related to the solid angle subtended by the spins surrounding the plaquette. Calculating the hoppings in the umbrella states, we find that hopping on the straight bonds is given by $t_1^s = e^{-s i \pi/4} (1 - s i \sin \delta) / \sqrt{2}$, with $|t_1^s| = \sqrt{(1 + \sin^2 \delta)/2} \equiv t_1$ and $\phi_1^s = \arctan(-s \sin \delta) - s\pi/4 \equiv \phi^s$ [see Fig. 1(c)]. In addition, hopping along the diagonal bonds is no longer 0 but $t_2 = -\sin \delta$, independent of chirality. Using these expressions we write the effective Hamiltonian for the electrons as

$$\begin{aligned} H^s(\mathbf{k}) &= \mathbf{d}(\mathbf{k}) \cdot \boldsymbol{\sigma} + d^0(\mathbf{k})\sigma^0, \quad \text{with} \quad (3) \\ d^0(\mathbf{k}) &= -2t_2 \cos k_x \cos k_y, \quad d^3(\mathbf{k}) = 2t_2 \sin k_x \sin k_y \\ d^1(\mathbf{k}) &= -2t_1 \cos \phi^s (\cos k_x + \cos k_y), \quad \text{and} \\ d^2(\mathbf{k}) &= -2t_1 \sin \phi^s (-\cos k_x + \cos k_y), \end{aligned}$$

where the two states referred to by the matrices are again the two sites of the unit cell and σ^0 is the unit matrix so that the Dirac Hamiltonian above is recovered for $\delta = 0$, implying $\phi^s = \pi/4$ and $t_2 = 0$. From the DOS [Fig. 2(b)] and the band structure [Fig. 3(a)], it is clear that finite $\delta \neq 0$ opens a gap for the Dirac cones. Since the hoppings are complex and the diagonal bonds have been activated, both time-reversal and parity symmetries are broken, allowing a QAH state [38]. To establish that the gapped state is indeed topologically non-trivial, we calculate the Chern number $C_n = \frac{1}{2\pi i} \oint_{\partial BZ} d\mathbf{k} \cdot \mathbf{A}(\mathbf{k})$, where $\mathbf{A}(\mathbf{k}) = \langle n\mathbf{k} | \nabla_{\mathbf{k}} | n\mathbf{k} \rangle$ is the Berry connection and find $C = \text{sgn}(t_2) \text{sgn}(\sin 2\phi^s)$. Chirality and Chern number hence perfectly correlate and we observe that inverting the magnetic polarization $\delta \rightarrow -\delta$ flips both the spin chirality and the Chern number. The off-diagonal Hall conductivity as a function of chemical potential, obtained from Eq. (3) for $\delta = 0.3$, is shown in Fig. 3(b). Figure 3(c-e) shows the effect of non-trivial topology on the edge of the system: chiral edge states connect valence and conduction band. As can be seen by comparing Figs. 3(d) and 3(e), the direction of the edge currents can be reversed by inverting the spin chirality. The latter can be easily manipulated by a small magnetic field.

The observation that spin configurations of the umbrella states are continuously connected to the coplanar flux phase suggests that the electronic QAH state can be understood from the low-energy physics at the Dirac points. We will demonstrate this by analyzing, in the spirit of Ref. [11], the system in a presence of an external magnetic field B and then take the limit of $B \rightarrow 0$. Focusing on the low-energy theory, $\delta\mathbf{k} = \mathbf{k} - \mathbf{M}_\gamma$ ($\gamma = \pm$), we introduce the magnetic field by way of a Peierls substitution $\hbar\delta\mathbf{k} \rightarrow \hat{\pi}$, where $\hat{\pi}$ is the dynamical momentum whose components satisfy the commutation relation $[\hat{\pi}_x, \hat{\pi}_y] = ieB\hbar$. We obtain two independent Hamiltonians for the two Dirac points, $H_\gamma = v_F(\hat{\pi}_\gamma^1 \sigma^x + \hat{\pi}_\gamma^2 \sigma^y) + m_\gamma \sigma^z$, which indeed has the appearance of the relativistic Dirac equation in a magnetic field. As can be seen by comparing to Eq. (3), our mass term $m_\gamma = 2\gamma t_2$ is a direct consequence of finite $t_2 = -\sin \delta$, and thus of finite chirality $\delta \neq 0$. Operators $\hat{\pi}_\gamma^1$ and $\hat{\pi}_\gamma^2$ are derived from $\hat{\pi}$ and satisfy the com-

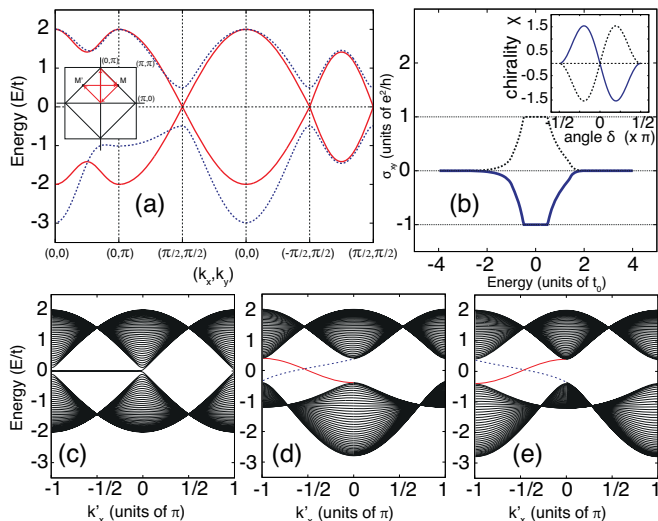


FIG. 3. (Color online) (a) The band structure of the gapless flux phase (red) and the insulating chiral phase (blue, $\delta = 0.3$) along a path in the Brillouin zone specified in the inset. (b) Quantized Hall conductivity in the chiral state ($\delta = 0.3$), when the Fermi level is in the gap, the quantized value depends on the chirality of the spin state. The inset shows the calculated chirality of the states Λ^\pm , where dashed (solid) corresponds to $+$ ($-$). (c-e) Spectrum of the flux phase calculated for a strip geometry, which explicitly shows the edge states at the open boundary. (c) π -flux phase ($\delta = 0.0$) exhibits edge states similar to graphene. (d,e) Chiral gapped phase ($\delta = 0.2$); chiral edge states connect valence and conduction bands. The states drawn with solid (dashed) lines lives on the top (bottom) edge. The chirality in (e) is reversed with respect to (d), the right- and left-moving states are consequently exchanged.

mutation relation $[\hat{\pi}_\gamma^1, \hat{\pi}_\gamma^2] = -i\gamma \sin(2\phi^s) eB\hbar$. Relativistic Dirac fermions in a magnetic field are known to exhibit zero modes in their spectrum [39], which cause the charge density imbalance in the ground state, potentially leading to an integer QAH effect. Here, the zero modes have energy $E_{0,\gamma} = -\gamma m_\gamma \text{sgn}(\sin 2\phi^s) \text{sgn}(eB)$, and the spectrum is asymmetric when m_+ and m_- have opposite sign. Following Haldane, we obtain the off-diagonal conductivity in the limit $B \rightarrow 0$, $\sigma_{xy} = \nu e^2/h$, where $\nu = \frac{1}{2} \text{sgn}(\sin 2\phi^s) [\text{sgn}(m_+) - \text{sgn}(m_-)] = \text{sgn}(t_2) \text{sgn}(\sin 2\phi^s)$. Hence, the gapped QAH umbrella state can be interpreted as Dirac fermions becoming massive, with masses of *opposite* sign, indeed, the $d^z(\mathbf{k})$ component of Eq. (3) has opposite sign at the two Dirac points $(\pm\pi/2, \pi/2)$. A sublattice potential, which also gaps out the Dirac fermions, would in contrast lead to equal masses, and the edge states would not cross the chemical potential.

Discussion and conclusions.— We investigated the interplay of itinerant electrons with a frustrated AFM spin background on the checkerboard lattice using Monte-Carlo methods. From the macroscopically degenerate *spin-ice* ground-state manifold, which optimizes the AFM interactions, the electron kinetic energy selects a unique magnetic ground state. The low-energy electronic states of the selected π -flux phase are given by a relativistic Dirac equation, and slightly stronger

kinetic energy induces a spin chirality, from which the Dirac fermions inherit a topologically nontrivial mass. The Kondo-lattice model on the checkerboard lattice thus provides a direct realization of Haldane’s proposal for obtaining a QAH state [11]. In addition, the QAH state’s chirality is coupled to a FM spin polarization and the direction of the edge currents can thus be switched by a magnetic field, an alluring property for quantum spintronics applications.

Our findings are also relevant in the broader context of fractionalization of quantum numbers in two different ways. First, the QAH state on the checkerboard lattice is actually a prominent candidates for hosting a *fractional* quantum-Hall-like state without a magnetic field, because the topologically nontrivial band can be made almost flat by tuning hoppings and flux [21, 40, 41]. It turns out that even if the flux and effective hoppings t_1 and t_2 that emerge in the “umbrella” configuration do not lead to very flat bands, additional longer-range hopping $-2t_3(\cos 2k_x + \cos 2k_y)$ can give a ratio of band gap vs. band width of ≈ 5 for $\delta = 0.3$, considerably less than ratios achievable by tuning all parameters [21] or in t_{2g} -orbital systems [42, 43], but comparable to e_g [42] systems or a square-lattice model [44]. Second, it was recently demonstrated that vortex defects of the localized magnetic order underlying a QAH state can carry fractional charge and spin quantum numbers in the electronic sector [45].

Acknowledgements.— This research was supported by the Interphase Program of the Dutch Science Foundation NWO/FOM (JV and JvdB) and by the Emmy-Noether program of the DFG (MD). SK acknowledges support from DST, India.

-
- [1] C. L. Kane and E. J. Mele, Phys. Rev. Lett. **95**, 146802 (2005).
 - [2] R. Roy, Phys. Rev. B **79**, 195322 (2009).
 - [3] J. E. Moore and L. Balents, Phys. Rev. B **75**, 121306 (2007).
 - [4] L. Fu, C. L. Kane, and E. J. Mele, Phys. Rev. Lett. **98**, 106803 (2007).
 - [5] Y. Xia, L. Wray, D. Qian, D. Hsieh, A. Pal, H. Lin, A. Bansil, D. Grauer, Y. S. Hor, R. J. Cava, and M. Z. Hasan, arXiv:0812.2078 (2008).
 - [6] D. Hsieh, Y. Xia, D. Qian, L. Wray, J. H. Dil, F. Meier, J. Osterwalder, L. Patthey, J. G. Checkelsky, N. P. Ong, A. V. Fedorov, H. Lin, A. Bansil, D. Grauer, Y. S. Hor, R. J. Cava, and M. Z. Hasan, Nature **460**, 1101 (2009).
 - [7] Y. Xia, D. Qian, D. Hsieh, L. Wray, A. Pal, H. Lin, A. Bansil, D. Grauer, Y. S. Hor, R. J. Cava, and M. Z. Hasan, Nature Physics **5**, 398 (2009).
 - [8] M. Koenig, S. Wiedmann, C. Bruene, A. Roth, H. Buhmann, L. W. Molenkamp, X.-L. Qi, and S.-C. Zhang, Science **318**, 766 (2007).
 - [9] K. von Klitzing, G. Dorda, and M. Pepper, Phys. Rev. Lett. **45**, 494 (1980).
 - [10] D. J. Thouless, M. Kohmoto, M. P. Nightingale, and M. den Nijs, Phys. Rev. Lett. **49**, 405 (1982).
 - [11] F. D. M. Haldane, Phys. Rev. Lett. **61**, 2015 (1988).
 - [12] C.-X. Liu, X.-L. Qi, X. Dai, Z. Fang, and S.-C. Zhang, Phys. Rev. Lett. **101**, 146802 (2008).

- [13] Y. Taguchi, Y. Oohara, H. Yoshizawa, N. Nagaosa, and Y. Tokura, *Science* **291**, 2573 (2001).
- [14] Y. Machida, S. Nakatsuji, Y. Maeno, T. Tayama, T. Sakakibara, and S. Onoda, *Phys. Rev. Lett.* **98**, 057203 (2007).
- [15] H. Takatsu, S. Yonezawa, S. Fujimoto, and Y. Maeno, *Phys. Rev. Lett.* **105**, 137201 (2010).
- [16] S. Raghun, X.-L. Qi, C. Honerkamp, and S.-C. Zhang, *Phys. Rev. Lett.* **100**, 156401 (2008).
- [17] I. Martin and C. D. Batista, *Phys. Rev. Lett.* **101**, 156402 (2008).
- [18] S. Kumar and J. van den Brink, *Phys. Rev. Lett.* **105**, 216405 (2010).
- [19] K. Ohgushi, S. Murakami, and N. Nagaosa, *Phys. Rev. B* **62**, R6065 (2000).
- [20] K. Sun, H. Yao, E. Fradkin, and S. A. Kivelson, *Phys. Rev. Lett.* **103**, 046811 (2009).
- [21] K. Sun, Z. Gu, H. Katsura, and S. Das Sarma, *Phys. Rev. Lett.* **106**, 236803 (2011).
- [22] S. Uebelacker and C. Honerkamp, *Phys. Rev. B* **84**, 205122 (2011).
- [23] X.-L. Qi, Y.-S. Wu, and S.-C. Zhang, *Phys. Rev. B* **74**, 085308 (2006).
- [24] S. T. Bramwell and M. J. P. Gingras, *Science* **294**, 1495 (2001).
- [25] L. D. C. Jaubert, S. Piatecki, M. Haque, and R. Moessner, *arXiv:1201.0677* (2012).
- [26] E. Dagotto, T. Hotta, and A. Moreo, *Phys. Rep. Rev.* **344**, 1 (2001).
- [27] R. Yu, S. Yunoki, S. Dong, and E. Dagotto, *Phys. Rev. B* **80**, 125115 (2009).
- [28] L. D. C. Jaubert, M. Haque, and R. Moessner, *Phys. Rev. Lett.* **107**, 177202 (2011).
- [29] I. Affleck and J. Marston, *Phys. Rev. B* **37**, 3774 (1988).
- [30] J. Lorenzana, G. Seibold, C. Ortix, and M. Grilli, *Phys. Rev. Lett.* **101**, 186402 (2008).
- [31] M. Yamanaka, W. Koshibae, and S. Maekawa, *Phys. Rev. Lett.* **81**, 5604 (1998).
- [32] D. Agterberg and S. Yunoki, *Phys. Rev. B* **62**, 13816 (2000).
- [33] H. Aliaga, B. Normand, K. Hallberg, M. Avignon, and B. Alascio, *Phys. Rev. B* **64**, 024422 (2001).
- [34] X. Chen, S. Dong, and J. M. Liu, *Phys. Rev. B* **81**, 064420 (2010).
- [35] A. H. Castro Neto, F. Guinea, N. M. R. Peres, K. S. Novoselov, and A. K. Geim, *Rev. Mod. Phys.* **81**, 109 (2009).
- [36] Y. Hatsugai, T. Fukui, and H. Aoki, *Phys. Rev. B* **74**, 205414 (2006).
- [37] Y. Kato, I. Martin, and C. D. Batista, *Phys. Rev. Lett.* **105**, 266405 (2010).
- [38] M. Onoda and N. Nagaosa, *J. Phys. Soc. Jpn.* **71**, 19 (2002).
- [39] R. Jackiw, *Phys. Rev. D* **29**, 2375 (1984).
- [40] D. N. Sheng, Z.-C. Gu, K. Sun, and L. Sheng, *Nature Communications* **2**, (2011).
- [41] N. Regnault and B. Bernevig, *Phys. Rev. X* **1**, 021014 (2011).
- [42] J. W. F. Venderbos, M. Daghofer, and J. van den Brink, *Phys. Rev. Lett.* **107**, 116401 (2011).
- [43] J. W. F. Venderbos, S. Kourtis, J. van den Brink, and M. Daghofer, *arXiv:1109.5955* (2011).
- [44] T. Neupert, L. Santos, C. Chamon, and C. Mudry, *Phys. Rev. Lett.* **106**, 236804 (2011).
- [45] R. A. Muniz, A. Rahmani, and I. Martin, *arXiv:1112.3347* (2011).